Construction of a Sensitive Bisphenol A Electrochemical Sensor based on Metal-organic Framework/Graphene Composites

Congming Li[1], Yanli Zhou[1,2,], Xu Zhu[2], Baoxian Ye[1], Maotian Xu[1,2,*]*

[1] College of Chemistry and Molecular Engineering, Zhengzhou University, Zhengzhou 450001, China
[2] Henan Key Laboratory of Biomolecular Recognition and Sensing, Shangqiu Normal University, College of Chemistry and Chemical Engineering, Shangqiu 476000, China
[*]E-mail: zhouyanli@mails.ucas.ac.cn (Y. Zhou); xumaotian@sqnu.edu.cn (M. Xu).

Bisphenol A (BPA), as a typical endocrine disruptor, has caused widespread concern in recent years, and its sensitive detection is particularly important. In this study, a sensitive BPA electrochemical sensor was fabricated using composites of copper-based metal-organic frameworks (Cu-MOFs) and electrochemically reduced graphene oxide (ERGO). The Cu-MOFs, ERGO, and Cu-MOFs/ERGO were characterized by scanning electron microscopy. Compared with the Cu-MOFs- or ERGO-modified electrode, the Cu-MOFs/ERGO-modified electrode displayed significantly enhanced electrocatalytic activity toward BPA. The prepared electrode displayed linear range from 0.02 µM to 90 µM and limit of detection of 6.7 nM (S/N=3) for BPA detection as shown by differential pulse voltammetry results under optimized conditions. Such good sensitivity could be ascribed to the synergistic catalysis from high adsorption and catalytic capacity of Cu-MOFs and to the excellent conductive property of ERGO. The Cu-MOFs/ERGO-modified electrode also exhibited high stability and anti-interference ability. The proposed sensor was successfully applied to determine BPA in plastic products. Thus, a promising and reliable tool is provided for the rapid analysis of emergency pollution caused by BPA.

1. INTRODUCTION

Bisphenol A [2,2-bis(4-hydroxyphenyl) propane, BPA] is one of the most important derivatives of phenol and acetone [1, 2]. This compound is widely employed as raw material in epoxy resins and polycarbonate plastics, such as food packaging, feeding bottles, water bottles, cans, and sports equipment [3, 4]. However, BPA, as a typical endocrine disruptor, can mimic estrogen and adversely affect the endocrine system of animals and human beings [5]. In addition, numerous studies have

demonstrated that BPA can also interfere with thyroid function, central nervous system, endocrine pancreas, immune system, and reproduction system even at very low part-per-trillion doses [6]. Therefore, accurate and sensitive detection of BPA is particularly important.

Various methods are used to determine BPA in different samples. These techniques include chromatography [7], spectrophotometry [8], immunoassay [9,10], chemiluminescence [11], and electrochemical sensor [12–26]. BPA is an electrochemical active compound. Thus, electrochemical methods are attractive for BPA detection because of the high sensitivity, simple operation, and onsite detection of these techniques. However, the signal-to-noise (S/N) of a bare electrode is insufficient to determine the trace level of BPA because of the high oxidation potential of this compound. Therefore, numerous studies have been conducted to explore for a breakthrough in electrode modification materials to improve the sensitivity of electrodes.

Metal–organic framework materials (MOFs), as a new class of hybrid inorganic–organic porous crystalline materials, have attracted considerable attention because of their extraordinarily high surface areas, tunable pore sizes, and adjustable internal surface properties. These materials are increasingly applied in gas adsorption and separation [27–31], catalysis [32,33], clean energy [34], drug delivery [35], imaging [36], magnetic and luminescent materials [37–40], and sensing [41–44]. Many sensors based on MOFs have been developed to detect some ions, small molecules, and other compounds. These MOFs have shown high selectivity and sensitivity. Copper-based MOFs (Cu-MOFs), as a robust electrochemical biosensing platform, have been immobilized using biomolecules of tyrosine and are used for BPA detection [25]. Three-dimensional Cu-MOFs provide large specific surface area and can adsorb numerous enzyme and BPA molecules, resulting in a sensitive and rapid biosensor for BPA detection. However, expensive or synthetic biomolecules were used in these MOF-based sensors. Thus, low-cost MOF-based materials with high catalytic activity should be developed for BPA detection.

Herein, nanosized Cu-MOFs-loaded graphene-film-modified glassy carbon electrode (Cu-MOFs/ERGO/GCE) was fabricated using electrochemical method. The electrode was used as a carrier to load more Cu-MOF nanoparticles because of the high surface areas of ERGO. The π–π stacking interactions between BPA and trithiocyanuric acid ligands in the MOFs improved the pre-enrichment of BPA on the electrode surface. Additionally, the Cu-MOFs played a key role as artificial mimetic catalysts in the electrooxidation of BPA at the Cu-MOFs/ERGO/GCE, which was electrochemically active because of the redox character of the Cu center. Therefore, compared with other modified electrode previously used for determining BPA, the Cu-MOFs improved the sensitivity, expanded the linear range, and lowered the limit of detection of the sensor. The electrochemical sensor was also applied to real samples to determine BPA, and satisfactory results were obtained.

2. EXPERIMENTAL

2.1. Chemicals and reagents

BPA, graphite powders, copper nitrate trihydrate ($CuSO_4 \cdot 3H_2O$), sodium hydroxide (NaOH), potassium permanganate ($KMnO_4$), sulfuric acid (H_2SO_4, 98%), sodium nitrate ($NaNO_3$), and

phosphoric acid (H_3PO_4) were obtained from Aladdin Chemistry Co., Ltd. (Shanghai, China). BPA was dissolved in ethanol (1×10^{-3} M) and kept at 4 °C in a refrigerator. All other reagents were of analytical grade and used without further purification. Phosphate-buffered saline (PBS, 0.1 M, pH 7.0) was prepared by mixing standard solutions of Na_2HPO_4 and NaH_2PO_4. Double distilled water (18 MΩ cm, Milli-Q gradient system, Millipore) was used for all solution preparation.

2.2. Instrumentation

Electrochemical measurements were performed on a CHI 660D electrochemical workstation (CH Instruments, China) with the modified GCE as working electrode, Pt wire as auxiliary electrode, and an Ag/AgCl electrode as reference electrode. All reported potentials were referred to the Ag/AgCl reference electrode. Scanning electron micrographs of the nanocomposite were recorded on a Quanta FEG 250 instrument. The measurements were performed at room temperature.

2.3. Synthesis of Cu-MOFs and GO

Cu-MOFs were synthesized as previously described with minor revision [44]. Briefly, 3.6 mmol of trithiocyanuric acid was dissolved in 12 mL of methanol under ultrasonic conditions, and 2.0 mmol of $CuSO_4 \cdot 3H_2O$ was dissolved in 12 mL of H_2O. Then, the $CuSO_4 \cdot 3H_2O$ solution was dropped into the above solution to obtain a homogeneous solution. The mixture was allowed to react for 2 h to produce orange precipitates. Finally, the obtained precipitates were extensively washed with water and methanol via centrifugation and dried under vacuum overnight.

Graphite oxide (GO) was synthesized from graphite powders according to a modified Hummer's method [15]. Graphite (1.0 g) and $NaNO_3$ (0.5 g) were successively added into concentrated H_2SO_4 (23 mL) in an ice bath, and the solution was continuously stirred for 1 h. Then, 3.0 g of $KMnO_4$ was slowly added into the solution. The solution was heated to 37 °C and kept at this temperature for 2 h. H_2O (80 mL) was thereafter added into the solution and heated to 95 °C. After 30 min, 50 mL of H_2O and 15 mL of H_2O_2 were added sequentially into the solution. The final suspension was filtered and washed thrice with 1% HCl and ultrapure water. The product was dried at vacuum to obtain GO. Then, appropriate amount of GO was dispersed into water to form 0.05 mg·mL^{-1} GO aqueous solution for further use.

2.4. Fabrication of Cu-MOFs/ERGO electrode

The surface of the GCE was mechanically polished by alumina powder (diameter: 0.05 μm) using a polishing cloth and then ultrasonically washed by anhydrous ethanol and ultrapure water. The electrode surface was dried with purified nitrogen stream. The synthesized Cu-MOFs nanoparticles (0.1 mg) were dispersed into 2.0 mL of 0.05 mg·mL^{-1} GO solution under ultrasonic conditions. Then, 5 μL of the mixed solution (Cu-MOFs and GO) was dropped onto the freshly cleaned GCE surface. After the electrode surface was dried in air, the Cu-MOFs/ERGO films were prepared by

electrochemical reduction in 0.1 M PBS at reduced potential window from -1.8 V to 0 V. Then, the obtained Cu-MOFs/ERGO/GCE was activated by cyclic scanning between 0.2 V and 1.1 V with rate of 0.10 V s^{-1} in above buffer solution to reach a steady state before use. The other electrodes, namely, ERGO/GCE and Cu-MOFs/GCE, were also prepared using the similar method.

2.5. Electrochemical behavior of BPA

Varying amounts of BPA were added into 5 mL of 0.1 M PBS (pH 7.0), and the oxidation current of BPA was determined by cyclic voltammetry (CV) and differential pulse voltammetry (DPV). CV measurements were performed with scanning range from 0.2 V to 1.1 V at a scan rate of 100 mV s^{-1}, and DPV was performed with pulse amplitude of 50 mV, pulse width of 50 ms, pulse time of 0.5 s, and rest time of 2 s.

2.6. Sample solution preparation

Plastic bags, disposable gloves, and water bottle bought from a local supermarket were processed to detect BPA in real plastic samples. First, the samples were cut into small pieces and washed several times with pure water. After drying at vacuum, 1.0 g of the plastic samples and 50 mL of ultrapure water were added into a flask and sealed with plastic wrap. Then, the mixture was heated at 70 °C for 48 h. Finally, the mixture was filtered with 0.45 μm filter membrane. The liquid product was collected and then diluted with 0.1 M PBS (pH 7.0) in a 50 mL volumetric flask. Otherwise, the spiked sample solution was prepared by the same method after adding a known amount of BPA standard solution.

3. RESULTS AND DISCUSSION

3.1. Characterization of Cu-MOFs/ERGO/GCE

Fig. 1 shows the scanning electron micrographs of ERGO, Cu-MOFs, and Cu-MOFs/ERGO composites. ERGO showed a typical wrinkle topography (Fig. 1a) with large surface area to load more Cu-MOFs nanoparticles. Fig. 1b shows the uniform nanosphere morphology of the synthesized Cu-MOFs with an approximate average diameter of 20 nm. In addition, Fig. 1c illustrates the uniform distribution of the Cu-MOFs nanoparticles in the ERGO sheets. The large surface area of Cu-MOFs and high conductivity of ERGO were expected to provide a high sensitive platform for electrochemical sensors.
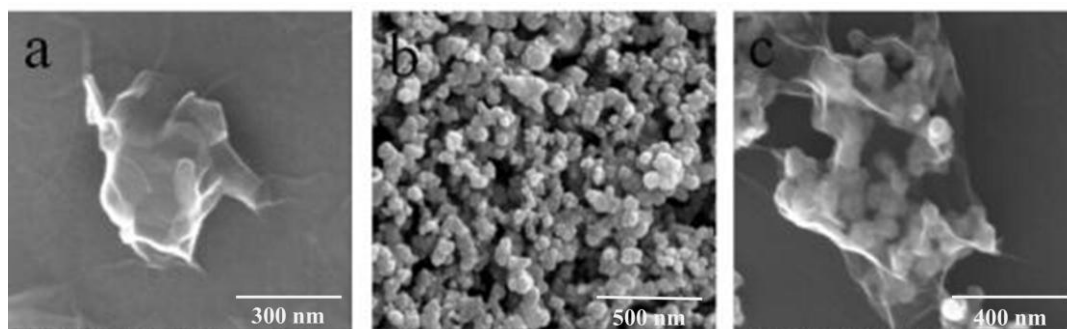
Figure 1. Scanning electron micrographs of (a) ERGO, (b) Cu-MOFs, and (c) Cu-MOFs/ERGO composites.

The surface properties of the different electrodes were characterized by CV in 1 mM $[Fe(CN)_6]^{3-/4-}$ solution (containing 0.1 M KCl). Fig. 2A shows the CVs of bare GCE and modified electrode. The electrochemical response of ferricyanide as a redox probe was a reversible process. For the bare GCE (curve a), a pair of well-separated redox peaks with peak separation (ΔE_p) of 0.078 V was observed. After modification with ERGO (curve b), the redox peak currents increased, but ΔE_p remained the same. These phenomena could be attributed to the excellent conductivity and large specific surface area of ERGO. However, the anodic and cathodic peaks almost completely disappeared in the Cu-MOFs/GCE (curve c) because of the poor electrical conductivity of the Cu-MOFs. After the modification of composites of Cu-MOFs and ERGO (curve d), the current peak increased compared with that of Cu-MOFs-modified electrode. Electrochemical impedance spectroscopy (EIS) was performed to investigate the electrode interface phenomena and electrode process dynamics. In the EIS, the Nyquist curve is the most common spectrum of electrochemical impedance. The curve consists of a semicircular high-frequency region and a low-frequency region of a linear part. This curve can be used to describe the interface properties of the electrode. R_{ct} is the semicircle diameter of impedance spectrum in the high-frequency range. Fig. 2B displays the Nyquist plots of the bare GCE, ERGO/GCE, Cu-MOFs/GCE, and Cu-MOFs/ERGO/GCE obtained in 5.0 mM $Fe(CN)_6^{3-/4-}$ containing 0.1 M KCl. The bare GCE exhibited a very small impedance (curve a), implying good electric conductivity. For the ERGO-modified electrode, the value of R_{ct} decreased, indicating that ERGO could accelerate the rate of the interfacial charge transfer. For Cu-MOFs/GCE, the semicircle diameter of the impedance drastically increased (curve c), because the MOFs, as the inert electron and mass transfer blocking layer, hindered the electron transfer of $Fe[(CN)_6]^{3-/4-}$. However, the R_{ct} value of Cu-MOFs/ERGO/GCE was smaller than that of Cu-MOFs/GCE because of the good electric conductivity of ERGO. These results indicate that the composites of Cu-MOFs/ERGO have been modified on the electrode surface, and the presence of graphene layer could enhance the electron transfer between electroactive species and electrode.
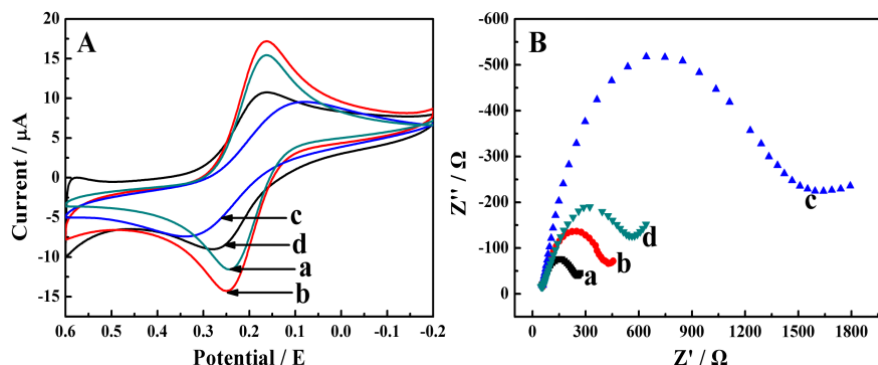
Figure 2. (A) Cyclic voltammograms of (a) bare GCE, (b) ERGO/GCE, (c) Cu-MOFs/GCE, and (d) Cu-MOFs/ERGO/GCE in 1.0 mM [Fe (CN)$_6$]$^{3-}$ containing 0.1 M KCl. Scan rate: 0.1 V·s^{-1}. (B) Electrochemical impedance spectra of the different electrodes: (a) GCE, (b) ERGO/GCE, (c) Cu-MOFs/GCE, and (d) Cu-MOFs/ERGO/GCE in 5.0 mM Fe(CN)$_6^{3-/4-}$ containing 0.1 M KCl. The frequency varied from 0.1 MHz to 0.01 Hz.

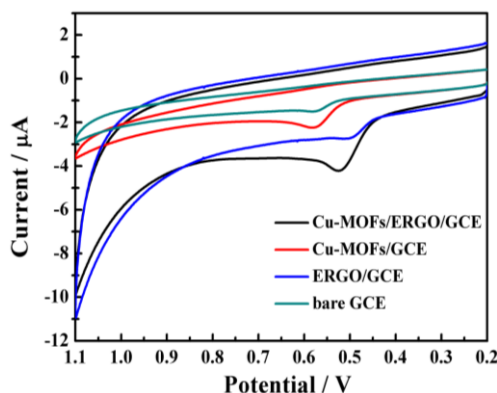*3.2. Voltammetric responses of BPA on the different electrodes*

Figure 3. Cyclic voltammograms of bare GCE, ERGO/GCE, Cu-MOFs/GCE and Cu-MOFs/ERGO/GCE in the presence of 50 µM BPA in 0.1 M PBS (pH 7.0).

The electrochemical behavior of BPA on the different electrodes was established by comparing the oxidation current and oxidation potential in 0.1 M PBS (pH 7.0) containing 50 µM BPA. Fig. 3 illustrates the CVs for the bare GCE, ERGO/GCE, Cu-MOFs/GCE, and Cu-MOFs/ERGO/GCE. An obvious oxidation peak of BPA was observed at approximately 0.55 V on all electrodes. No corresponding reduction peak appeared in the reverse scan. This result indicated the irreversibility of the electrochemical oxidation process of BPA. Compared with the bare electrode, the peak current of BPA on the ERGO/GCE and Cu-MOFs/GCE increased slightly. The peak current on the Cu-MOFs/ERGO/GCE increased significantly, which indicated that the combination of ERGO and Cu-MOFs nanoparticles obviously improved the electrochemical response of BPA on the electrode surface. The electron transfer rate between BPA and the modified electrode was greatly accelerated because of the high conductivity of ERGO, the catalytic active sites on Cu-MOFs, and the π–π stacking interactions between BPA and Cu-MOFs. Thus, the electrocatalysis of electrode for BPA oxidation was effectively improved.

3.3. Optimization of experimental conditions

It is well known that the type and pH of electrolytes have different effects on the determination of analytes. So we evaluate the electrochemical response of BPA on the Cu-MOFs/ERGO/GCE by CV in different electrolytes. The influence of different supporting electrolytes, such as acetic acid-sodium acetate buffer solution (HAc-NaAc), tris-hydroxylamine-hydrochloric acid buffer solution (Tris-Hcl), Britton-Robinson buffer solution (BR), and PBS were investigated in the presence of 50 µM BPA (Fig. 4). The results showed that the BPA in PBS exhibited the best peak shape and peak current. Hence, 0.1 M PBS was used for further experiments.
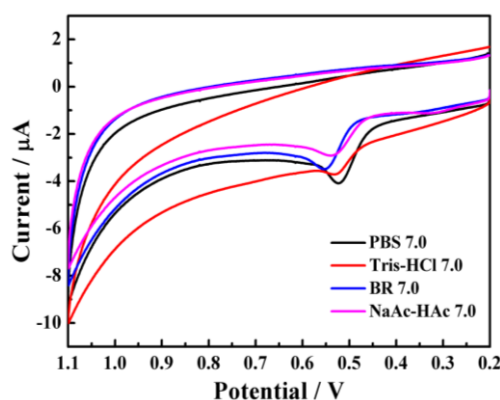

Figure 4. Cyclic voltammograms of the Cu-MOFs/ERGO/GCE in the presence of 50 µM BPA in different supporting electrolytes at 0.1 M (HAc-NaAc, Tris-Hcl, BR and PBS).
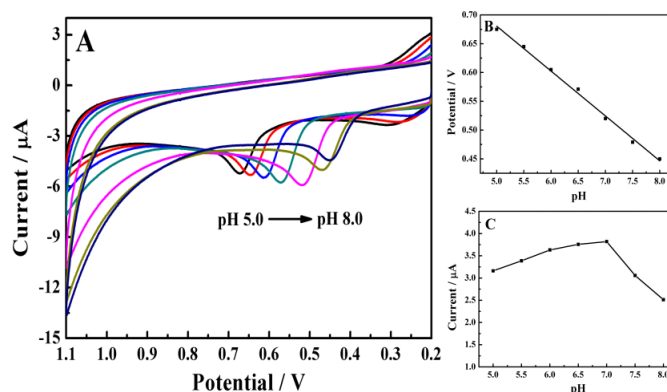

Figure 5. (A) Cyclic voltammograms of the Cu-MOFs/ERGO/GCE in the presence of 50 µM BPA in 0.1 M PBS at different pH values: 5.0, 5.5, 6.0, 6.5, 7.0, 7.5, and 8.0; (B) The relationship between the different pH values and peak potential in 0.1 M PBS; (C) The relationship between the different pH and peak current in 0.1 M PBS.

Then, the influence of different pH values of PBS on the voltammetric behavior of BPA was also investigated (Fig. 5A). Thus, PBS with pH values ranging from 5.0 to 8.0 were chosen. The peak current gradually increased as the pH change from 5.0 to 7.0, and then decreased as the value exceeded

7.0 (Fig. 5B). The 0.1 M PBS (pH 7.0), at which the peak current reached the maximum, was selected as the blank solution. Peak potential shifted toward the negative direction with increase in pH, which demonstrated the participation of the proton transfer in the electrode process (Fig. 5C). A good linear relationship was obtained between the peak potential (E_p) and solution pH (Fig. 5B). The linear regression equation was E_p (V) = - 0.068 pH + 1.07 (R=0.995). The slope of 0.068 V per unit of pH was close to the theoretical value of 0.059 V. This result indicated that the protons and electrons had a ratio of 1:1 in the electrode reaction of BPA. This finding is consistent with the oxidation of BPA [15].

3.4. Electrochemical behavior of BPA on the Cu-MOFs/ERGO/GCE

The effect of scan rate on the response of BPA at the Cu-MOFs/ERGO/GCE was evaluated by varying the scan rate (v) from 0.10 V s^{-1} to 0.45 V s^{-1} in 0.01 M PBS, and the superimposed voltammograms are shown in Fig. 6A. The oxidation peak potential shifted positively, and the peak currents increased with increasing sweep rate. Moreover, the peak current was linearly proportional to the scan rate from 0.10 V s^{-1} to 0.45 V s^{-1} (Fig. 6B), and the linear regression equation was as follows: I_p (µA) = 4.994 v + 2.47 (R = 0.996). The results demonstrated that the electrode process of BPA was adsorption-controlled. That is, BPA underwent a surface electrochemical reaction at the Cu-MOFs/ERGO/GCE.
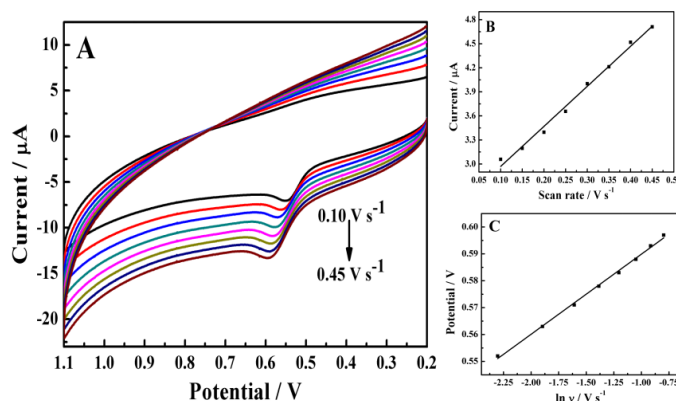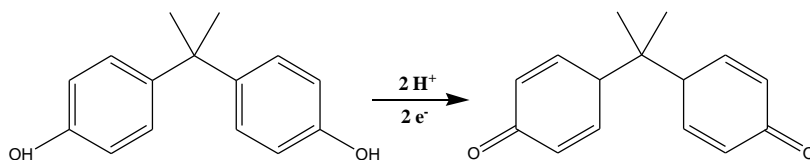

Figure 6. (A) Cyclic voltammograms of the Cu-MOFs/ERGO/GCE in the presence of 50 µM BPA in 0.1 M PBS (pH 7.0) at different scan rates: 0.10, 0.15, 0.20, 0.25, 0.30, 0.35, 0.40 and 0.45 V s^{-1}; (B) Relationship between peak potential and different scan rates; (C) The relationship between the peak potential and natural logarithm of scanning rates for BPA.

In addition, The oxidation peak potential shifts positively with increasing scan rate, and as shown in Fig. 6C, there is a linear correlation between the peak potential and the natural logarithm of scan rate (E_p = 0.620 + 0.029 ln$v$, R = 0.997). For the irreversible electrode process, the relationship between E_p and ln$v$ obey the following equation [26]:

$$E_P(V) = E^{0'} + \frac{RT}{\alpha nF} \ln \frac{RTk_s}{\alpha nF} + \frac{RT}{\alpha nF} \ln v$$

where $E^{0'}$ is the formal potential, k_s is the electrochemical rate constant, n_α is the number of the electron transferred in the rate determining step, α is the transfer coefficient, T is the temperature, F is

the Faraday constant, and *T*, *F* and *R* have their usual meanings (T = 298 K, F = 96487 C mol^{-1} and R = 8.314 J mol^{-1} K^{-1}) . We could obtain the value of αn_α from the slope (0.029) of the above equation. αn_α was calculated to be 0.90. For most systems, the value of α is from 0.3 to 0.7. Thus, assuming α = 0.5, then n_α was estimated to be 2.0 for the oxidation of BPA on the Cu-MOFs/ERGO electrode. Moreover, the number of proton in the oxidation of BPA equal the number of electrons (E_p (V) = -0.078 pH + 1.07). Based on above results, the electrode reaction of BPA on the Cu-MOFs/ERGO/GCE was an adsorption driven two-electron and two-proton process. The electro-oxidation mechanism of BPA is schematically expressed in Scheme 1, and the detailed electro-oxidation process could be expressed as follows:
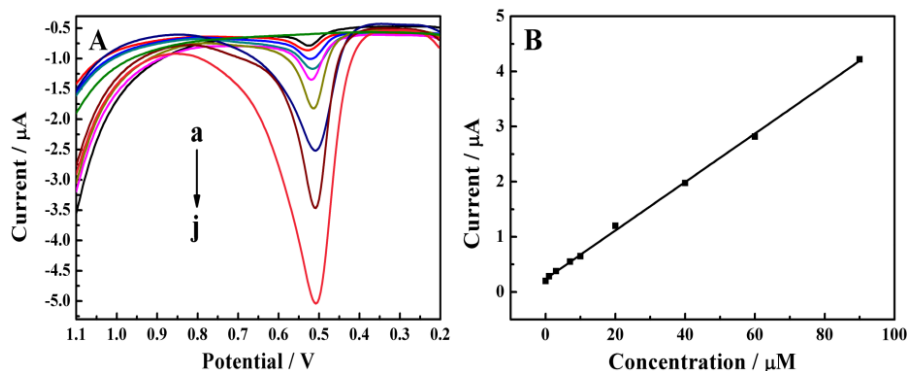

Scheme 1. A proposed electrode reaction equation of BPA at Cu-MOFs/ERGO/GCE.

3.5. Analytical performances

A series of BPA solutions with different concentrations were analyzed under the optimal experimental conditions. The performance of the Cu-MOFs/ERGO-based sensor in detecting BPA was investigated by DPV. Fig. 7A shows the change in peak current with different concentrations of BPA. Fig. 7B indicated the good linear relationship of the peak currents with the different BPA concentrations from 0.02 μM to 90 μM. The linear regression equation was I_{pa} (μA) = 0.0439 c + 0.236 (μM) (R = 0.999) with low limit detection of 6.7 nM (S/N=3). Moreover, we compared the analytical parameters of the prepared sensor with other BPA sensors as illustrated in Table 1 [12-26]. Only a few examples of BPA aptasensors with lower limit have been reported [17-22]. However, the construction of these aptasensors was complex and time-consuming, the practicality of the developed system was difficult to ensure. For the enzyme modified electrodes [23-25], the limit detection was not low enough, and the expensive enzyme molecules were utilized. Moreover, enzyme activity was not good to maintain in the wider pH range, which resulted the difficulty in the application in the real samples. For other MOF-based materials, high catalytic activity could be obtained for BPA detection [26]. Nevertheless, the additional cationic surfactant as a preconcentration reagent was needed to modify on the surface of the Ce-MOFs. Compared with other several nanomaterials [12-16], the Cu-MOFs/ERGO composites showed higher or comparative sensitivity because of the significantly enhanced electrocatalytic activity toward BPA. Such good electrocatalytic activity could be ascribed to the synergistic catalysis from high adsorption and catalytic capacity of Cu-MOFs and excellent conductive property of ERGO. In addition, the enzyme-like effect of the Cu-MOFs/ERGO composites greatly promoted the electrocatalytic oxidation of BPA.

Table 1. Comparison of the linear ranges and limits of detection of the different BPA sensors

Electrode material	Linear range (M)	Limit of detection (M)	Reference
Pt/Gr/CNTs/GCE	$6.0×10^{-8}$–$8.0×10^{-5}$	$4.2×10^{-8}$	12
AuPdNPs/GNs/GCE	$5.0×10^{-8}$–$1.0×10^{-5}$	$8.0×10^{-9}$	13
AuNPs/SGNF/GCE	$8.0×10^{-8}$–$2.5×10^{-4}$	$3.5×10^{-8}$	14
Cu_2O/rGO/GCE	$1.0×10^{-7}$–$8.0×10^{-5}$	$5.3×10^{-8}$	15
TiO_2/AuNTAs electrode	$1.0×10^{-7}$–$3.89×10^{-5}$	$6.2×10^{-9}$	16
Aptamer/MCH/GNPs/GR/GCE	$1.0×10^{-8}$–$1.0×10^{-5}$	$5.0×10^{-9}$	17
Aptamer/NPGF/GCE	$1.0×10^{-10}$–$1.0×10^{-7}$	$5.6×10^{-11}$	18
Poly(pyrroleNTA)/Cu^{2+}/Aptamer/ GCE	$1.0×10^{-11}$–$1.0×10^{-6}$	$1.0×10^{-11}$	19
MB-P/MCH/Fc-P/Au electrode	$1.0×10^{-12}$–$1.0×10^{-10}$	$1.9×10^{-13}$	20
MCH/Aptamers/AuNPs/BDD electrode	$1.0×10^{-14}$–$1.0×10^{-9}$	$7.2×10^{-15}$	21
Aptamer/MWCNTs/AuNPs/Au electrode	$1.0×10^{-10}$–$1.0×10^{-8}$	$5.0×10^{-11}$	22
Tyr-diazonium-MWCNTs/BDD electrode	$1.0×10^{-11}$–$1.0×10^{-7}$	$1.0×10^{-11}$	23
Tyr/silk peptide/graphene/GCE	$2.0×10^{-9}$–$5.48×10^{-6}$	$7.2×10^{-10}$	24
Cu-MOFs/Tyr/Chit/GCE	$5.0×10^{-8}$–$3.0×10^{-6}$	$1.3×10^{-8}$	25
CTAB/Ce-MOFs/GCE	$5.0×10^{-9}$–$5.0×10^{-6}$, $5.0×10^{-6}$–$5.0×10^{-5}$	$2.0×10^{-9}$	26
Cu-MOFs/ERGO/GCE	$2.0×10^{-8}$–$9.0×10^{-5}$	$6.7×10^{-9}$	This Work

Figure 7. (A) DPV curves of increasing concentration of BPA in 0.1 M PBS (pH 7.0) using the electrochemical sensor (a–j: 0.02, 1.0, 3.0, 7.0, 10.0, 20.0, 40.0, 60.0, 90.0 μM); (B) Relationship of the peak current with the target concentration.

The reproducibility and stability of the Cu-MOFs/ERGO/GCE was evaluated by the measurement of the response to 50 μM BPA in 0.1 M PBS by DPV. We prepared eight different BPA sensors with the same modifications of 5 μL of Cu-MOFs/ERGO composites. Reproducibility within

mean value of ± 5% was generally achieved. After the modified electrodes were stored in a refrigerator at 4 °C for one week, 94.5% of the initial current signal was obtained. After two weeks of storage, 89.2% signal remained, indicating the good long-term stability of the as-prepared sensor. In addition, common inorganic ions (such as 100-fold Ca^{2+}, Mg^{2+}, Na^+, SO_4^{2-}, CO_3^{2-}, NO^{3-}, Cl^-, HPO_4^{2-}, $H_2PO_4^-$, and Ac^-) and organic solvents (such as 0.25% v/v acetone, acetonitrile, methanol, and ethanol) showed no influence on the determination of BPA. The Cu-MOFs/ERGO/GCE exhibited excellent performance for BPA determination because of the well-dispersed, high-yield, clean surface, and synergistic effect of Cu-MOFs/ERGO composite, as well as the large surface area, high conductivity of the ERGO.

3.6. Real sample analysis

Table 2. Determination of BPA in food package using Cu-MOFs/ERGO/GCE

Samples	This method (μM)	HPLC (μM)	Added (μM)	Detected (μM)	RSD (%)	Recovery (%)
Plastic bags	0.67	0.68	4.0	4.6	1.19	98.46
Disposable gloves	0.35	0.36	5.0	5.36	3.45	100.22
Water bottle	not detectable	not detectable	8.0	8.43	5.38	105.38

We determined the BPA content in real samples through a recovery study using the analytical procedure in section 3.7 to evaluate the performance of Cu-MOFs/ERGO/GCE in practical analytical application. Table 2 shows the determination results of BPA in plastic samples. High-performance liquid chromatography (HPLC) was also employed to further demonstrate the accuracy of the proposed electrode. Table 2 shows that the recovery of BPA was over the range from 98.46% to 105.38%, and the RSD (n=3) was from 1.19% to 5.38%. These results indicated that the proposed electrochemical sensor based on Cu-MOF/ERGO composites was stable, effective, and accurate for practical applications.

4. CONCLUSIONS

In summary, we have successfully constructed a simple and sensitive approach for detecting BPA using an electrochemical sensor based on Cu-MOFs/ERGO composites. The integration of Cu-MOFs and ERGO may greatly improve the active sites, effective area, and electrochemical response of the modified electrode, because of the high surface, excellent conductivity, and great electrocatalytic activity of the Cu-MOFs/ERGO composites. The proposed sensor displayed excellent sensitivity, good selectivity, reproducibility, and stability. Satisfactory results were obtained when this method was applied to determine BPA in real samples. Therefore, Cu-MOFs/ERGO/GCE can be applied to other plastic products.

References

1. W. Dekant, W. Völkel, *Toxicol. Appl. Pharm.*, 228 (2008) 114-134.
2. W. Volkel, T. Colnot, G.A. Csanady, *Chem. Res. Toxicol.*, 15 (2002) 1281-1287.
3. J. Michałowicz, *Environ. Toxicol. Phar.*, 37 (2014) 738-758.
4. N. Olea, R. Pulgar, P. Pérez, F. Olea-Serrano, A. Rivas, A. Novillo-Fertrell, V. Pedraza, A.M. Soto, C. Sonnenschein, *Environ. Health Persp.*, 104 (1996) 298-305.
5. H. Sambe, K. Hoshina, K. Hosoya, J. Haginaka, *J. Chromatogr. A*, 1134 (2006) 16-23.
6. J.R. Rochester, *Reprod. Toxicol.*, 42 (2013) 132-155.
7. R. Lu, J.Z. Fang, G.H. Liu, J.Q. Zhang, Z. Zhu, H.G. Liu, K. Lin, H.M. Zhang, S.Y. Lu, *Anal. Bioanal. Chem.*, 408 (2016) 2621-2629.
8. R. Zhang, L.N. Zhao, R.T. Liu, *J. Photochem. Photobiol. B*, 163 (2016) 40-46.
9. C.J. Hou, L.X. Zhao, F.L. Geng, D. Wang, L.H. Guo, *Anal. Bioanal. Chem.*, 408 (2016) 8795-8804.
10. J. Wan, Y.X. Si, C. Li, K. Zhang, *Anal. Methods*, 8 (2016) 3333-3338.
11. C. Lu, J.G. Li, Y. Yang, J.M. Lin, *Talanta*, 82 (2010) 1576-1580.
12. Z.X. Zheng, Y.L. Du, Z.H. Wang, Q.L. Feng, C.M. Wang, *Analyst*, 138 (2013) 693-701.
13. B.Y. Su, H.L. Shao, N. Li, X.M. Chen, Z.X. Cai, X. Chen, *Talanta*, 166 (2017) 126-132.
14. X.L. Niu, W. Yang, G.Y. Wang, J. Ren, H. Guo, J.Z. Gao, *Electrochim. Acta*, 98 (2013) 167-175.
15. R.G. Shi, J. Liang, Z.S. Zhao, A.F. Liu, Y. Tian, *Talanta*, 169 (2017) 37-43.
16. L.S. Hu, C.C. Fong, X.M. Zhang, L.L. Chan, P.K.S. Lam, P.K. Chu, K.Y. Wong, M.S. Yang, *Environ. Sci. Technol.*, 50 (2016) 4430-4438.
17. L. Zhou, J.P. Wang, D.J. Li, Y.B. Li, *Food Chem.*, 162 (2014) 34-40.
18. Y. Zhu, C.Q. Zhou, X.P. Yan, Y. Yan, Q. Wang, *Anal. Chim. Acta*, 883 (2015) 81-89.
19. L.S. Hu, C.C. Fong, X.M. Zhang, L.L. Chan, P.K.S. Lam, P.K. Chu, K.Yin. Wong, M.S. Yang, *Environ. Sci. Technol.*, 50 (2016) 4430-4438.
20. I. Kazane, K. Gorgy, C. Gondran, N. Spinelli, A. Zazoua, E. Defrancq, S. Cosnier, *Anal. Chem.*, 88 (2016) 7268-7273.
21. P. Yu, Y.Q. Liu, X.H. Zhang, J.W. Zhou, E.H. Xiong, X.Y. Li, J.H. Chen, *Biosen. Bioelectron.*, 79 (2016) 22-28.
22. Y.B. Ma, J.S. Liu, H.D. Li, *Biosen. Bioelectron.*, 92 (2017) 21-25.
23. N. Zehani, P. Fortgang, M.S. Lachgar, A. Baraket, M. Arab, S.V. Dzyadevych, R. Kherrat, N. Jaffrezic-Renault, *Biosens. Bioelectron.*, 74 (2015) 830-835.
24. Y. Qu, M. Ma, Z. Wang, G. Zhan, B. Li, X. Wang, H. Fang, H. Zhang, C. Li, *Biosens. Bioelectron.*, 44 (2013) 85-88.
25. X. Wang, X.B. Lu, L.D. Wu, J.P. Chen, *Biosen. Bioelectron.*, 65 (2015) 295-301.
26. J. Zhang, X.J. Xu, L. Chen, *Sensor. Actuat. B*, DOI: org/10.1016/j.snb.2018.01.170.
27. J.R. Li, R.J. Kuppler, H.C. Zhou, *Chem. Soc. Rev.*, 38 (2009) 1477-1504.
28. Y. Zhao, M. Seredych, Q. Zhong, T.J. Bandosz, *ACS Appl. Mater. Interfaces*, 5 (2013) 4951-4959.
29. M.P. Suh, H.J. Park, T.K. Prasad, D.W. Lim, *Chem. Rev.*, 112 (2012) 782-835.
30. K. Sumida, D.L. Rogow, J.A. Mason, T.M. McDonald, E.D. Bloch, Z.R. Herm, T.H. Bae, J.R. Long, *Chem. Rev.*, 112 (2012) 724-781.
31. Z.R. Herm, E.D. Bloch, J.R. Long, *Chem. Mater.*, 26 (2014) 323-338.
32. M. Yoon, R. Srirambalaji, K. Kim, *Chem. Rev.*, 112 (2012) 1196-1231.

33. H.G.T. Nguyen, N.M. Schweitzer, C.Y. Chang, T.L. Drake, M.C. So, P.C. Stair, O.K. Farha, J.T. Hupp, S.T. Nguyen, *ACS Catal.*, 4 (2014) 2496-2500.
34. S.L. Li, Q. Xu, *Energy Environ. Sci.*, 6 (2013) 1656-1683.
35. P. Horcajada, C. Serre, G. Maurin, N.A. Ramsahye, F. Balas, M. Vallet-Regí, M. Sebban, F. Taulelle, G. Ferey, *J. Am. Chem. Soc.*, 130 (2008) 6774-6780.
36. D. Liu, K. Lu, C. Poon, W. Lin, *Inorg Chem.*, 53 (2013) 1916-1924.
37. W.G. Yang, G.Y. Zhang, W. Weng, B. Qiu, L.H. Guo, Z.Y. Lin, G.N. Chen, *RSC Adv.*, 4 (2014) 58852-58857.
38. Z. Hu, W.P. Lustig, J. Zhang, C. Zheng, H. Wang, S.J. Teat, Q. Gong, N.D. Rudd, J. Li, *J. Am. Chem. Soc.*, 137 (2015) 16209-16215.
39. Y.X. Guo, X. Feng, T.Y. Han, S. Wang, Z.G. Lin, Y.P. Dong, B. Wang, *J. Am. Chem. Soc.*, 136 (2014) 15485-15488.
40. K.S. Asha, K. Bhattacharyya, S. Mandal, *J. Mater. Chem. C*, 2 (2014) 10073-10081.
41. L.E. Kreno, K. Leong, O.K. Farha, M. Allendorf, R.P. Van Duyne, J.T. Hupp, *Chem. Rev.*, 112 (2012) 1105-1125.
42. S.K. Bhardwaj, N. Bhardwaj, G.C. Mohanta, P. Kumar, A.L. Sharma, K.H. Kim, A. Deep, *ACS Appl. Mater. Interfaces*, 7 (2015) 26124-26130.
43. Y. Zhang, X. Bo, A. Nsabimana, C. Han, M. Li, L. Guo, *J. Mater. Chem. A*, 3 (2015) 732-738.
44. T.Z. Liu, R. Hu, X. Zhang, K.L. Zhang, Y. Liu, X.B. Zhang, R.Y. Bai, D.L. Li, Y.H. Yang, *Anal. Chem.*, 88 (2016) 12516-12523.